Journal of Pharmaceutical Analysis 12 (2022) 617–626

Contents lists available at ScienceDirect

Journal of Pharmaceutical Analysis

journal homepage: www.elsevier.com/locate/jpa

Original article

Preparation of Fe_3O_4@SW-MIL-101-NH_2 for selective pre-concentration of chlorogenic acid metabolites in rat plasma, urine, and feces samples

Shi-Jun Yin [a], Xi Zhou [a], Li-Jing Peng [a], Fang Li [b], Guo-Can Zheng [b], Feng-Qing Yang [a, *], Yuan-Jia Hu [c, **]

[a] Department of Pharmaceutical Engineering, School of Chemistry and Chemical Engineering, Chongqing University, Chongqing, 401331, China
[b] Analytical and Testing Center, Chongqing University, Chongqing, 401331, China
[c] State Key Laboratory of Quality Research in Chinese Medicine, Institute of Chinese Medical Sciences, University of Macau, Macao, 999078, China

ARTICLE INFO

Article history:
Received 13 September 2021
Received in revised form
23 January 2022
Accepted 24 January 2022
Available online 31 January 2022

Keywords:
Sandwich structure
Metal-organic framework
Chlorogenic acid
Magnetic solid-phase extraction
Metabolic pathway

ABSTRACT

An innovative sandwich-structural Fe-based metal-organic framework magnetic material (Fe_3O_4@SW-MIL-101-NH_2) was fabricated using a facile solvothermal method. The characteristic properties of the material were investigated by field emission scanning electron microscopy, transmission electron microscopy (TEM), energy-dispersive X-ray spectroscopy, Fourier transform infrared spectroscopy, X-ray powder diffraction, vibrating sample magnetometry, and Brunauer-Emmett-Teller measurements. Fe_3O_4@SW-MIL-101-NH_2 is associated with advantages, such as robust magnetic properties, high specific surface area, and satisfactory storage stability, as well as good selective recognition ability for chlorogenic acid (CA) and its metabolites via chelation, hydrogen bonding, and π-interaction. The results of the static adsorption experiment indicated that Fe_3O_4@SW-MIL-101-NH_2 possessed a high adsorption capacity toward CA and its isomers, cryptochlorogenic acid (CCA) and neochlorogenic acid (NCA), and the adsorption behaviors were fitted using the Langmuir adsorption isotherm model. Then, a strategy using magnetic solid-phase extraction (MSPE) and ultra-performance liquid chromatography coupled with quadrupole time-of-flight tandem mass spectrometry (UPLC-Q-TOF MS/MS) was developed and successfully employed for the selective pre-concentration and rapid identification of CA metabolites in rat plasma, urine, and feces samples. This work presents a prospective strategy for the synthesis of magnetic adsorbents and the high-efficiency pretreatment of CA metabolites.

1. Introduction

Chlorogenic acid (CA), synthesized in plants via the esterification of caffeic and quinic acids during aerobic respiration, is usually found in traditional Chinese medicines, such as burdock, dandelion, honeysuckle, *Chrysanthemum indicum*, and hawthorn [1,2], as well as in various natural products, such as coffee, plums, and potatoes [3,4]. Predominant activities of CA, such as antioxidant and anti-inflammatory effects, have attracted the attention of researchers [5]. Modern pharmacological studies have shown that CA possesses many biological activities [6,7], including cholagogic, antibacterial, hypotensive [8], anti-cancer [9], and anti-AIDS effects [10]. Moreover, CA is an important raw material in food, drug, cosmetic, and other industries [11].

The metabolic fate of CA in various biological samples has been studied using ultra-high-performance liquid chromatography coupled with quadrupole time-of-flight mass spectrometry (UPLC-Q-TOF MS) [12]. Nevertheless, the direct determination of the metabolites of CA in complex biological samples is usually difficult because of the complicated biological matrix interferences and low concentration of structurally similar metabolites. Therefore, to separate metabolites from complex matrices and obtain a high detection sensitivity, sample pretreatment procedures are indispensable. To date, the most widely used sample pretreatment methods for metabolism studies are liquid-liquid microextraction, solid-phase extraction (SPE) (C_{18} SPE column, hydrophilic-lipophilic balance

Peer review under responsibility of Xi'an Jiaotong University.
* Corresponding author.
** Corresponding author.
E-mail addresses: fengqingyang@cqu.edu.cn (F.-Q. Yang), yuanjiahu@um.edu.mo (Y.-J. Hu).

https://doi.org/10.1016/j.jpha.2022.01.002

column), and solid-phase microextraction [13–17]. However, these methods have some inherent weaknesses, including time-consuming, complicated procedures, high organic solvent consumption, and low selectivity. Thus, the development of efficient and reliable sample pretreatment techniques with short extraction equilibration time and high selectivity to target analytes is an essential prerequisite for the highly efficient detection of metabolites.

Recently, magnetic solid-phase extraction (MSPE), a pre-enrichment procedure for concentrating target analytes from complex samples by applying an external magnetic field and magnetic adsorbent [18,19], has received significant attention owing to its low cost, fast separation, and targeting ability [20,21]. Although various materials [22,23], such as metallic oxides, carbon nanotubes [24,25], polydopamine, covalent organic frameworks, cyclodextrin, and surfactants, have been used as modifying agents for the synthesis of magnetic sorbents for MSPE, the synthesis of new magnetic adsorbents for achieving high adsorption capacity and binding specificity is still highly desired. Metal-organic frameworks (MOFs), a type of porous coordination polymers formed by the self-assembly of metal ions or metal clusters with bridged ligands through coordination bonds [26,27], are associated with advantages, such as large surface area, high porosity, tunable pore size, controllable morphology, and simple functionalization [28,29]. These unique properties make MOFs ideal MSPE adsorbents. At present, two types of MOF-based magnetic materials are commonly used [30]. With respect to the core-shell structure material [31], the large mass proportion of Fe_3O_4 limits its adsorption capacity. Furthermore, the use of acids as modulation agents, which can regulate the crystal structure, should be avoided in order to protect magnetic nuclei during the material preparation process. Another common type of MOF-based magnetic material is MOF surface modified by Fe_3O_4 using the co-precipitation method [32], but the magnetic property of the adsorbent is easily lost during repeated use due to the weak connection between Fe_3O_4 and MOF. In addition, although MSPE has been widely employed in the pre-concentration of water pollutants, heavy metal ions, pesticide residues, endogenous hormones, and natural active compounds, the use of MSPE in metabolic studies of CA has not been reported.

Therefore, in the present study, a novel sandwich-structured Fe-based MOF magnetic material (Fe_3O_4@SW-MIL-101-NH_2) was prepared using a facile and sustainable process for the MSPE of CA based on its interaction with Fe(III) to form CA-Fe(III) complexes [33,34]. The Fe_3O_4 nanoparticles were modified on the surface of MIL-101-NH_2 by the dropwise addition of dispersed Fe_3O_4, and then MIL-101-NH_2 was further modified on Fe_3O_4@MIL-101-NH_2 to prepare Fe_3O_4@SW-MIL-101-NH_2 using the solvothermal method. The synthesized material has a large specific surface area, abundant binding sites, and stable magnetic properties. Furthermore, CA and its isomers, cryptochlorogenic acid (CCA) and neochlorogenic acid (NCA), were selected as target analytes to study the optimal adsorption-desorption conditions, adsorption mechanism, repeatability, stability, and analytical performance of the proposed method. Finally, the Fe_3O_4@SW-MIL-101-NH_2/MSPE and UPLC-Q-TOF MS/MS analysis were successfully used for the selective pre-concentration and rapid identification of CA metabolites in rat plasma, urine, and feces samples.

2. Materials and methods

2.1. Materials and reagents

Ferric chloride hexahydrate ($FeCl_3 \cdot 6H_2O$, purity>98%), NaCl, KH_2PO_4, K_2HPO_4, *N*,*N*-dimethylformamide (DMF, purity>99%), and acetic acid (AA, purity>99%) were purchased from ChengDu Chron Chemicals Co., Ltd. (Chengdu, China). Fe_3O_4 was purchased from Shanghai Macklin Biochemical Co., Ltd. (Shanghai, China). 2-aminoterephthalic acid (H_2BDC-NH_2, purity≥98%) was purchased from Shanghai DiBai Biotechnology Co., Ltd. (Shanghai, China). CA (purity≥98%) was purchased from Chengdu Herb Substance Co., Ltd. (Chengdu, China). CCA (purity≥98%) and NCA (purity≥98%) were purchased from Chengdu Desite Biological Technologies Co., Ltd. (Chengdu, China), and their chemical structures are shown in Fig. S1. The water used for all the experiments was purified using a water purification system (ATSelem 1820A, Antesheng Environmental Protection Equipment Co., Ltd., Chongqing, China). All the solvents used in high-performance liquid chromatography (HPLC) analysis, such as methanol (MeOH) and acetonitrile (ACN), were of HPLC-grade and purchased from Adamas-beta (Shanghai, China).

2.2. Preparation of Fe_3O_4@SW-MIL-101-NH_2

Fe_3O_4@SW-MIL-101-NH_2 was synthesized using a facile three-step strategy. MIL-101-NH_2 was prepared by the solvothermal method according to Guo et al. [35] with some modifications. $FeCl_3 \cdot 6H_2O$ (4 mM) and H_2BDC-NH_2 (4 mM) were added and well dispersed in DMF (90 mL) in a 250 mL flask under sonication for 0.5 h. Then, 3.6 mL of AA was added and stirred for another 0.5 h. The mixture was stirred uniformly and sealed in a teflon-lined autoclave. The autoclave was heated to 110 °C and maintained for 24 h. The prepared MIL-101-NH_2 were centrifugally separated, washed with DMF (50 mL for twice) and ethanol (50 mL for twice), and dried under vacuum at 60 °C for 12 h.

Fe_3O_4 was immobilized on the surface of MIL-101-NH_2 using the following procedure. First, 100 mg of MIL-101-NH_2 was dispersed into 15 mL of DMF and ultrasonicated for 0.5 h at room temperature (approximately 25 °C). Then, 15 mL of Fe_3O_4 (0.6 mM) was added to the suspension at room temperature and stirred at 500 r/min. Finally, the sediments were collected using an external magnet, washed with 30 mL of DMF three times and re-dispersed in 12 mL of DMF.

In the last procedure, H_2BDC-NH_2 (4 mM) and $FeCl_3 \cdot 6H_2O$ (4 mM) were dissolved in DMF (3 mL) as solution A. Then, 4 mL of Fe_3O_4@MIL-101-NH_2 and 1 mL of solution A were mixed and heated at 120 °C and stirred for 8 h. MIL-101-NH_2 grew uniformly on the surface of the precursor material. The resultant Fe_3O_4@SW-MIL-101-NH_2 was collected by using an external magnet and washed with 30 mL of DMF three times. Subsequently, it was dried under vacuum at 60 °C for 12 h. The instruments and conditions for the characterization of the materials are described in the Supplementary data.

2.3. Sample preparation

Information on animal administration is provided in the Supplementary data. The blood was collected from the fundus venous plexus with heparin sodium tubes at 0–0.5 h, 0.5–4 h and 4–8 h after administration. The urine and feces samples were collected at 0–4 h and 4–8 h after administration. Plasma was obtained using centrifugation at 2259 *g* for 10 min at 4 °C. The feces samples were suspended in MeOH (200 mg of feces sample:1.0 mL of MeOH) through ultrasonic extraction for 10 min. Then, the suspension liquid was treated by centrifugation at 2259 *g* for 20 min and the supernatant was collected. All samples were stored at −20 °C for further extraction and analysis.

2.4. Magnetic solid-phase extraction procedure

The Fe_3O_4@SW-MIL-101-NH_2 adsorbent (2 mg) was added to the sample solution (pH 5.0). The MSPE process was performed at 30 °C in a temperature-controlled air bath shaker (SHZ-82, Jintan Hongke Instrument Factory, Jintan, China) for 7.5 min at 180 r/min. An external magnet was then used to assist the separation of the

adsorbed analytes from the sample solution. The analytes were then eluted by dispersion of the adsorbent in a mixed solution containing 0.8 mL of Na_3PO_4 (50 mM) and 0.2 mL of MeOH, which was assisted by ultrasonication for 5 min. Subsequently, the eluate was isolated from the adsorbent with the aid of an external magnet and collected in a 1.5 mL centrifuge tube. Finally, the resulting desorption solution was filtered through a 0.22 μm filter (Shanghai Titan Scientific Co., Ltd., Shanghai, China) before being injected into the high-performance liquid chromatography (HPLC) or ultra-performance liquid chromatography-electrospray ionization with quadrupole-time of flight tandem mass spectrometry technology (UPLC-ESI-Q-TOF MS/MS) system for analysis. The detailed chromatographic conditions are shown in the Supplementary data.

3. Results and discussion

3.1. Characterization of Fe_3O_4@SW-MIL-101-NH_2

The morphology and structure of the prepared MIL-101-NH_2, Fe_3O_4@MIL-101-NH_2, and Fe_3O_4@SW-MIL-101-NH_2 were studied thoroughly using scanning electron microscopy (SEM) and transmission electron microscopy (TEM) (Fig. 1). Fig. 1A shows a micrograph of MIL-101-NH_2, which presents a regular octahedron with a smooth surface. Furthermore, the combination of Fe_3O_4 and MIL-101-NH_2 resulted in uniformly dispersed Fe_3O_4 spheres on MIL-101-NH_2, resulting in the rough surface of the material (Figs. 1B and C). Fig. 1D shows the SEM image of the Fe_3O_4@SW-MIL-101-NH_2, which clearly shows that the regular octahedral structure was maintained. As shown in Fig. 1E, Fe_3O_4 agglomerated on the outer surface of MIL-101-NH_2. However, it can be seen that part of the Fe_3O_4 was shed after the ultrasonic preparation of the TEM sample, a procedure that is detrimental to the reuse of the materials. Moreover, TEM revealed that the Fe_3O_4 were firmly fastened onto Fe_3O_4@SW-MIL-101-NH_2 (Fig. 1F). With the same ultrasonic treatment, no significant shedding of Fe_3O_4 was observed. In addition, the mapping and energy-dispersive X-ray spectrometer results in Figs. 1G and H confirmed the presence of C, N, O, and Fe.

The presence of functional groups on the material was investigated using Fourier transform infrared (FT-IR) spectroscopy (Fig. 2A). The strong adsorption peak in the 3500–3200 cm^{-1} region is

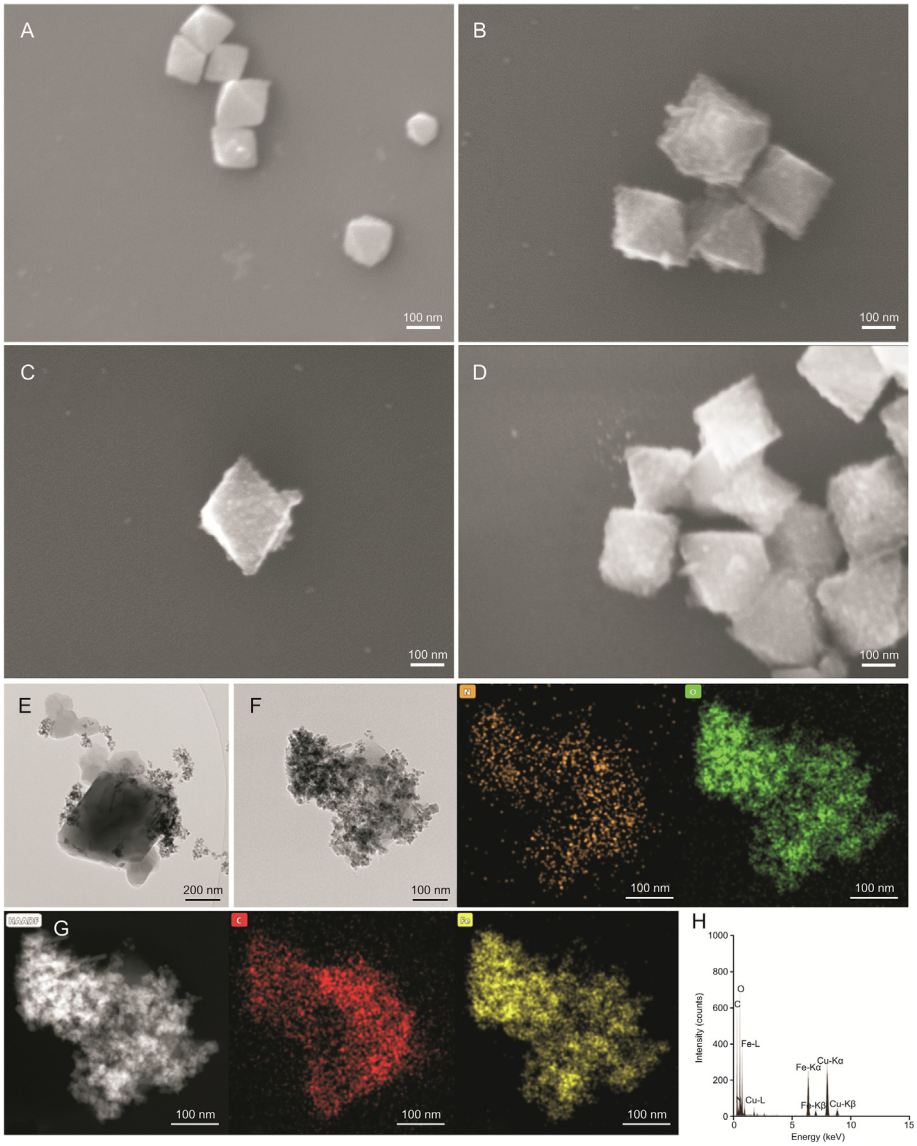

Fig. 1. Scanning electron microscopy (SEM) images of (A) MIL-101-NH_2, (B and C) Fe_3O_4@MIL-101-NH_2, and (D) Fe_3O_4@SW-MIL-101-NH_2; transmission electron microscopy (TEM) images of (E) Fe_3O_4@MIL-101-NH_2 and (F) Fe_3O_4@SW-MIL-101-NH_2; (G and H) energy-dispersive X-ray spectroscopy results of the main elements.

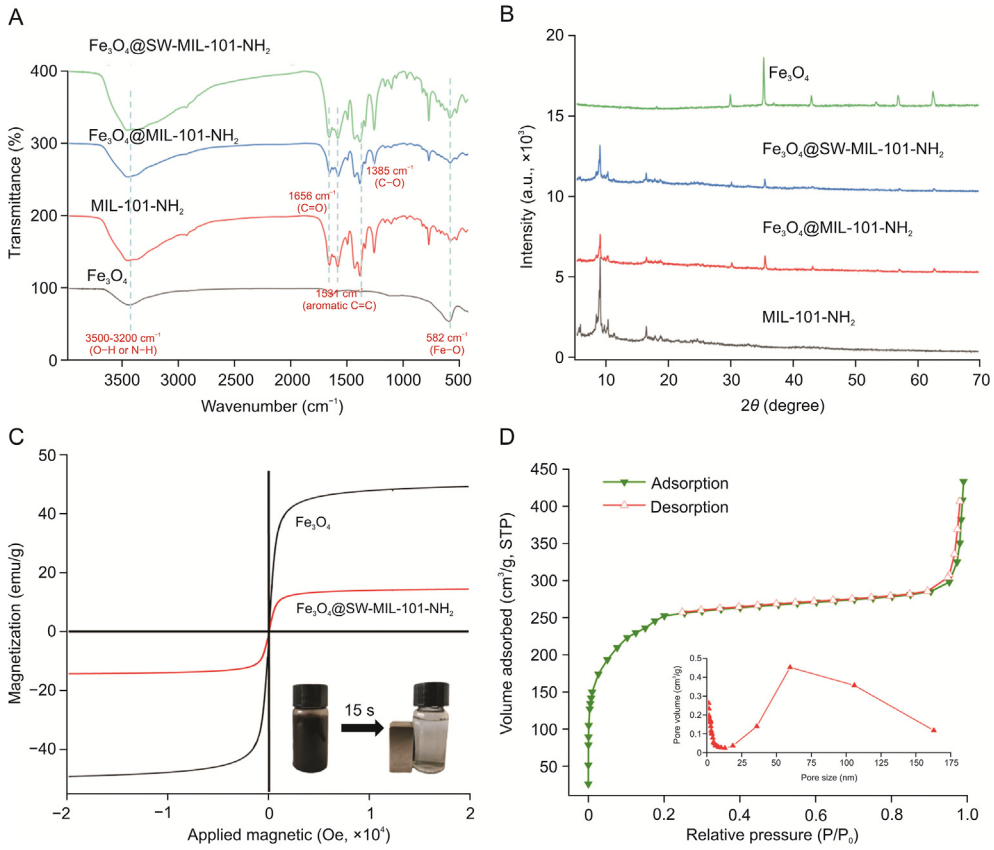

Fig. 2. (A) The Fourier transform infrared (FT-IR) spectra and (B) X-ray diffraction (XRD) of Fe_3O_4, MIL-101-NH_2, Fe_3O_4@MIL-101-NH_2 and Fe_3O_4@SW-MIL-101-NH_2. (C) Magnetization hysteresis loops of Fe_3O_4 and Fe_3O_4@SW-MIL-101-NH_2. The inset picture is the disperse state of the Fe_3O_4@SW-MIL-101-NH_2 adsorbent in aqueous solution and under an external magnetic force. (D) Nitrogen adsorption-desorption isotherm of Fe_3O_4@SW-MIL-101-NH_2; inset shows the pore-size distribution of Fe_3O_4@SW-MIL-101-NH_2.

attributed to the O–H stretching vibration of the hydroxyl group on the Fe_3O_4 surface or the N–H asymmetrical and symmetrical stretching vibration of the amino group [36,37]. The characteristic absorption peaks observed at 1450–1600 cm^{-1} and 1531 cm^{-1} were attributed to the benzene skeleton and aromatic C=C bonds. The adsorption peaks at 1656 cm^{-1} and 1385 cm^{-1} were assigned to the C=O and O=C–O stretching of the carboxylic groups [38]. As can be seen in the FT-IR spectrum of Fe_3O_4, the single absorption peak at 582 cm^{-1} is attributed to Fe–O stretching [39], proving that Fe_3O_4 were successfully anchored on MIL-101-NH_2. For Fe_3O_4@SW-MIL-101-NH_2, the adsorption peaks of MIL-101-NH_2 were significantly enhanced (compared to Fe_3O_4@MIL-101-NH_2), but no new absorption peaks appeared, indicating that the MIL-101-NH_2 shell layer was successfully wrapped. As shown by the X-ray diffraction (XRD) patterns (Fig. 2B), the six characteristic peaks at $2\theta = 30.0°$, 35.2°, 42.9°, 53.6°, 56.7°, and 62.4° can be attributed to Fe_3O_4, a finding that is in agreement with the Fe_3O_4 standard (JCPDS, No. 65–3107). As can be seen in the XRD patterns of Fe_3O_4@SW-MIL-101-NH_2 and Fe_3O_4@-MIL-101-NH_2, the characteristic peaks at $2\theta = 4.0°–20.0°$ are attributed to the crystalline MIL-101(Fe) with a face-centered cubic structure [40].

A vibrating sample magnetometer (VSM) was used to measure the magnetic properties of Fe_3O_4@SW-MIL-101-NH_2 and Fe_3O_4 at about 25 °C. The magnetic behavior of the materials was identified based on the VSM curve (Fig. 2C). The magnetic hysteresis curves of Fe_3O_4 and Fe_3O_4@SW-MIL-101-NH_2 indicated that the magnetization saturations of Fe_3O_4 and Fe_3O_4@SW-MIL-101-NH_2 were 49.1 and 14.3 emu/g, respectively. Although the modification of SW-MIL-101-NH_2 resulted in partial loss of magnetism compared to Fe_3O_4, it was sufficient for the saturation magnetization of the Fe_3O_4@SW-MIL-101-NH_2 adsorbent to complete the fast magnetic separation under an external magnetic field. The inset of Fig. 2C illustrates that the adsorbent could be completely collected from a uniformly dispersed solution within 15 s. Nitrogen adsorption-desorption isotherms were obtained to evaluate the surface area and porous structure of Fe_3O_4@SW-MIL-101-NH_2 (Fig. 2D). The adsorption-desorption isotherm can be classified as type II isotherms with an H_3-type hysteresis loop, indicating the existence of particle aggregates with pore networks [41]. In addition, the Brunauer-Emmett-Teller specific surface area was 901.4 m^2/g, which can be attributed to the fact that the complete octahedral shape of the material is maintained during synthesis. The Barrett-Joyner-Halenda average pore width was 50 Å, and the pore volume was 0.67 cm^3/g.

3.2. Optimization of MSPE conditions

To achieve the optimum extraction efficiency, several adsorption-desorption conditions were systematically studied and optimized, including amount of adsorbent, extraction time, ion strength (NaCl and KH_2PO_4–K_2HPO_4), pH value, and extraction temperature (adsorption conditions), as well as elution solvent and elution time (desorption conditions). The MSPE parameters for the extraction of CA, CCA, and NCA of Fe_3O_4@SW-MIL-101-NH_2 were investigated by changing one variable at a time during optimization. All experiments were performed in triplicate. In addition, the HPLC method used in the quantitative analysis was developed and validated (Table S1).

A suitable adsorbent amount for MSPE performance is important for obtaining a high extraction efficiency. Therefore, different adsorbent amounts (0.5–3 mg) were investigated. Fig. 3A shows that the

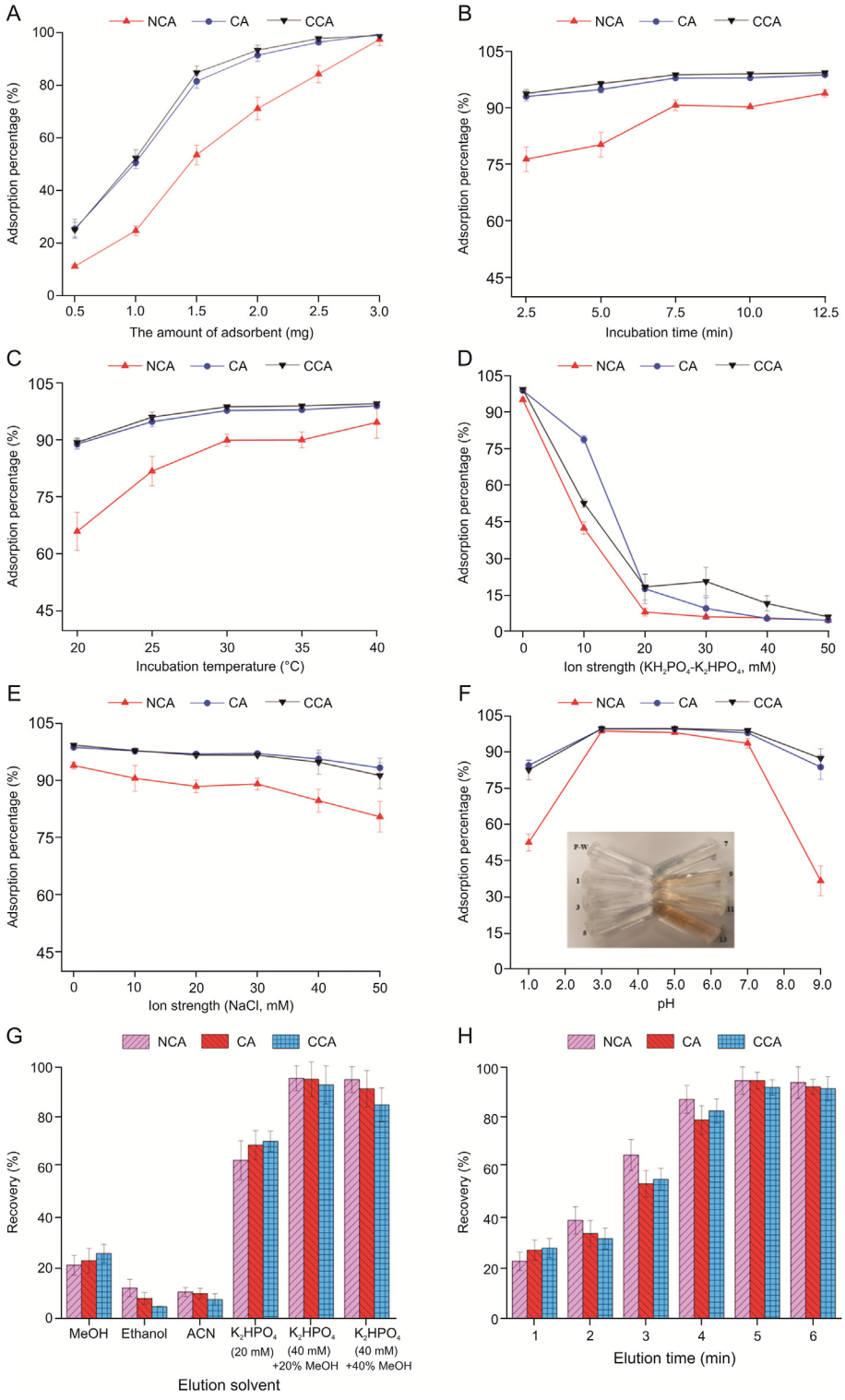

Fig. 3. Effects of (A) the amount of adsorbent, (B) extraction time, (C) extraction temperature, (D) ion strength (KH_2PO_4–K_2HPO_4), (E) ion strength (NaCl), (F) pH value (10.0 mM NaOH–HCl), and mixed reference compounds solutions at different pH conditions (inset) on the adsorption percentage. Effects of (G) elution solvent type and (H) elution time on the recovery of analytes using Fe_3O_4@SW-MIL-101-NH_2 as an adsorbent. CA: chlorogenic acid; CCA: cryptochlorogenic acid; NCA: neochlorogenic acid.

extraction efficiencies of CA, CCA, and NCA were enhanced by increasing the adsorbent amount. To facilitate the optimization of other conditions, 2 mg was selected for the subsequent study. Furthermore, the effects of 2.5–12.5 min extraction time on extraction efficiency were studied. The extraction efficiency gradually improved with the increase in extraction time and reached the highest at 7.5 min (Fig. 3B). Therefore, 7.5 min was selected for further studies. The rapid adsorption of the analytes may be ascribed to the high specific surface area and porous structure of the adsorbent.

The effect of extraction temperature on the extraction efficiency was assessed over a temperature range of 20–40 °C. The extraction efficiency exhibited a remarkable increase from 20 to 30 °C and

became steady with a further increase in temperature (Fig. 3C). For minimal energy consumption and satisfactory extraction efficiency, an extraction temperature of 30 °C was chosen. The effect of ionic strength was investigated by adding NaCl or KH_2PO_4–K_2HPO_4 to the tested solution in a concentration range of 0–50.0 mM. However, the addition of salt had a negative effect on the extraction efficiency (Figs. 3D and E). The viscosity of the aqueous solution increased with the addition of salt, which resulted in difficulty during mass transfer. Furthermore, the addition of salt also reduced the interaction of analytes with the sorbent surface, thereby reducing the extraction efficiency. In addition, for the KH_2PO_4–K_2HPO_4 system (Fig. 3D), the extraction efficiency declined sharply with the increase in salt concentration, which may be attributed to the competition of phosphate groups on the adsorption sites by chelation. Hence, chelation may be the primary interaction between CA, CCA, NCA, and the adsorbent, and no salt was added to the samples in the subsequent experiments.

The pH value of the sample solution plays an important role in the adsorption of the target analytes onto the adsorbent because it can regulate the surface charge species and density, as well as the stability of the adsorbent and analytes. Different pH values (1.0–9.0) were evaluated for the extraction of CA, CCA, and NCA by the adsorbent. The extraction efficiency increased with an increase in the pH value of 3.0–5.0, but decreased at a pH of 5.0–9.0 (Fig. 3F). These results can be attributed to the following factors: 1) The pKa values of CA, CCA, and NCA are approximately 3.59 (Table S2), when the pH > pKa, the presence of target analytes in molecular form will facilitate their adsorption on Fe_3O_4@SW-MIL-101-NH_2. When the pH was 3.0, the analytes could be ionized, weakening their adsorption. Furthermore, the nitrogen atoms of amino groups (−NH_2) are protonated at low pH, and the H-bond and dipolar-dipolar interactions between the adsorbent and analytes are also weakened. 2) At a slightly acidic pH (pH 5.0), surface complexation can be formed through a combination of acidic hydroxyl (−OH) groups and carboxyl (−COOH) groups of analytes and positive charge sites (Fe^{3+}) on the adsorbent. However, at a high acidic pH, excessive H^+ can lead to the protonation of hydroxyl and carboxyl groups, reducing the electron donor and coordination capacity of O atoms. 3) As shown in the inset of Fig. 3F, the solution gradually turns dark yellow when the pH is 7.0–13.0, which indicates that the analyte is stable under acidic conditions and unstable under neutral and alkaline conditions. The degradation of the analytes increases with an increase in alkalinity. In addition, NCA presents a faster degradation rate because it can be isomerized into CA and CCA [42]. Therefore, a pH value of 5.0 was selected as the optimum condition.

The type of elution solvent is a significant factor that influences the extraction recovery. Three different solvents, namely, ACN, MeOH, and ethanol, were compared. The results (Fig. 3G) indicate that MeOH has a better elution recovery; therefore, KH_2PO_4 (20 mM), KH_2PO_4 (40 mM)-20% MeOH, and KH_2PO_4 (40 mM)-40% MeOH were further investigated. As shown in Fig. 3G, the elution solvent KH_2PO_4 (40 mM)-20% MeOH had the highest recovery. This may be because KH_2PO_4 and MeOH have the capability to compete for binding sites for complexation and hydrogen bonding, respectively. Therefore, KH_2PO_4 (40 mM)-20% MeOH was selected as the appropriate desorption solvent. In addition, the influence of desorption time was investigated in the range of 1–6 min. The results (Fig. 3H) confirmed that 5 min is enough to elute the analytes from the Fe_3O_4@SW-MIL-101-NH_2 adsorbent.

3.3. Static adsorption

The concentration-dependent adsorption capacity was determined to investigate the binding ability of Fe_3O_4@SW-MIL-101-NH_2. The equilibrium adsorption concentration of the analytes (c_e, μg/mL) in the collected supernatant was measured by HPLC analysis. The equilibrium adsorption capacity (Q_e, mg/g) was calculated using the following equation:

$$Q_e = \frac{c_o - c_e}{m} \times V$$

where C_o (μg/mL) is the initial concentration, m (g) is the mass of the Fe_3O_4@SW-MIL-101-NH_2 adsorbent, and V represents the volume of the analyte solution.

The equilibrium isotherms (Fig. S2) were obtained using different initial analyte concentrations (25–400 μg/mL) under the optimized adsorption conditions. The Q_e value increased remarkably with an increase in the initial concentration from 25 to 200 μg/mL, and then reached saturation adsorption at 400 μg/mL. The experimental results showed that the maximum adsorption capacities of the adsorbents for CA, CCA, and NCA were 39.5, 43.9, and 15.6 mg/g, respectively. Furthermore, two adsorption isotherm models, Langmuir and Freundlich, were employed to investigate the binding properties of the adsorbent. As shown in Table 1 and Fig. S3, the adsorption isotherms of Fe_3O_4@SW-MIL-101-NH_2 can be better described by the Langmuir model, and their R^2 values are higher than 0.99, indicating that the surface of the material is homogeneous with a predominant chemical adsorption mechanism. In addition, the Q_{max} values calculated from the Langmuir equations were very close to the Q_e values obtained from the experiments.

3.4. Reusability and storage stability

Reusability is a crucial parameter for evaluating the stability and efficiency of an adsorbent. To examine the reusability of the adsorbent, Fe_3O_4@SW-MIL-101-NH_2 was vortexed twice sequentially with deionized water after desorption of the target analytes, and the dried adsorbent was introduced into another adsorption-desorption cycle. As shown in Fig. S4A, the adsorbent can be reused at least 12 times without significant loss of extraction efficiency (<5%) and magnetism. The storage stability of the adsorbent is an important factor for practical applications, which was investigated by using the adsorbents for 42 days of storage at room

Table 1
The linear relationship and parameters of Langmuir and Freundlich adsorptions.

Compounds	Langmuir				Freundlich			
	Regressive equation	Q_{max} (mg/g)	K_l (mL/mg)	R^2	Regressive equation	K_f $mg\left(^{1-\frac{1}{n}}\right)\frac{1}{L^{n}g^{-1}}$	$\frac{1}{n}$	R^2
NCA	$Y = 0.143X + 0.065$	15.4	0.45	0.992	$Y = 0.093X + 2.245$	175.8	0.09	0.949
CA	$Y = 0.084X + 0.027$	37.0	0.32	0.994	$Y = 0.219X + 2.550$	354.8	0.22	0.957
CCA	$Y = 0.100X + 0.023$	43.5	0.23	0.998	$Y = 0.233X + 2.576$	376.7	0.23	0.939

$0.1 < 1/n \leq 0.5$ represents that the adsorption is very easy to perform; $0.5 < 1/n \leq 1$ represents that the adsorption is easy to perform; $1 > 1/n$ represents that the adsorption is difficult to perform. CA: chlorogenic acid; CCA: cryptochlorogenic acid; NCA: neochlorogenic acid.

Table 2
Mass spectrometry and chromatography information of chlorogenic acid and its metabolites.

No.	Retention time (min)	Formula	$[M-H]^-$ (*m/z*)			MS/MS fragment ion	Metabolic pathway	Real samples						
			Theoretical	Experimental	Error (mDa)			Feces		Plasma			Urine	
								0–4 h	4–8 h	0.5 h	4 h	8 h	0–4 h	4–8 h
C0	15.952	$C_{16}H_{18}O_9$	353.3046	353.1407	−0.46	353.1407 ($[M-H]^-$), 190.9291 ($[M-H-C_9H_6O_3]^-$), 178.9049 ($[M-H-C_7H_{10}O_5]^-$), 135.1120 ($[M-H-C_7H_{10}O_5-CO_2]^-$)	Parent (CA)	+	+	+	+	+	+	+
C1	13.550	$C_9H_8O_4$	179.1518	179.1082	−0.24	179.1082 ($[M-H]^-$), 135.1371 ($[M-H-CO_2]^-$), 117.7631 ($[M-H-CO_2-OH]^-$), 93.0342 ($[M-H-CO_2-C_2H_2O]^-$)	Hydrolysis to caffeic acid	−	−	+	+	+	−	−
C2	12.969	$C_{11}H_{10}O_5$	221.1889	221.1540	−0.16	221.1540 ($[M-H]^-$), 179.1226 ($[M-H-C_2H_2O]^-$)	Acetylation of C1	+	+	+	+	+	+	+
C3	13.536	$C_{11}H_{11}NO_5$	236.2036	236.1730	−0.13	236.1730 ($[M-H]^-$), 162.0954 ($[M-H-C_2H_4NO_2]^-$), 93.0336 ($[M-H-C_5H_5NO_4]^-$)	Glycine conjugation of C1	−	+	+	+	+	+	+
C4	16.141	$C_{16}H_{18}O_9$	353.3046	353.2109	−0.27	353.2109 ($[M-H]^-$), 190.9096 ($[M-H-C_9H_6O_3]^-$), 178.9049 ($[M-H-C_7H_{10}O_5]^-$), 135.1120 ($[M-H-C_7H_{10}O_5-CO_2]^-$)	4-caffeoylquinic acid	+	+	+	+	+	+	+
C5	17.095	$C_{16}H_{20}O_9$	355.3204	355.1577	−0.46	355.1577 ($[M-H]^-$), 191.2094 ($[M-H-C_9H_8O_3]^-$)	Reduction	+	+	+	+	+	+	+
C6	17.083	$C_{15}H_{18}O_{10}$	357.2930	357.1599	−0.37	357.1599 ($[M-H]^-$), 181.0272 ($[M-H-C_6H_8O_6]^-$)	Glucuronidation of C1 and reduction	+	+	−	−	−	−	−
C7-1	14.321	$C_{17}H_{20}O_9$	367.3314	367.2422	−0.24	367.2422 ($[M-H]^-$), 193.2617 ($[M-H-C_7H_{10}O_5]^-$), 191.2581 ($[M-H-C_{10}H_8O_3]^-$), 173.2477 ($[M-H-C_{10}H_8O_3-H_2O]^-$), 134.0059 ($[M-H-C_9H_{13}O_7]^-$)	Methylation	+	+	+	+	+	+	+
C7-2	16.872	$C_{17}H_{20}O_9$	367.3314	367.2422	−0.24	367.2422 ($[M-H]^-$), 193.2617 ($[M-H-C_7H_{10}O_5]^-$), 191.2581 ($[M-H-C_{10}H_8O_3]^-$), 173.2477 ($[M-H-C_{10}H_8O_3-H_2O]^-$), 134.0059 ($[M-H-C_9H_{13}O_7]^-$)	Methylation	+	+	+	+	+	+	−
C8-1	17.586	$C_{16}H_{18}O_{10}$	369.3040	369.1726	−0.36	369.1732 ($[M-H]^-$), 192.9726 ($[M-H-C_6H_8O_6]^-$), 134.0127 ($[M-H-C_6H_8O_6-C_2H_3O_2]^-$)	Methylation and glucuronidation of C1	+	+	+	+	+	+	−
C8-2	17.809	$C_{16}H_{18}O_{10}$	369.3040	369.1727	−0.36	369.1727 ($[M-H]^-$), 193.0284 ($[M-H-C_6H_8O_6]^-$), 149.1840 ($[M-H-C_6H_8O_6-CO_2]^-$)	Methylation and glucuronidation of C1	−	−	−	−	−	−	+
C8-3	7.426	$C_{16}H_{18}O_{10}$	369.3040	369.1732	−0.35	369.1726 ($[M-H]^-$), 193.0281 ($[M-H-C_6H_8O_6]^-$), 149.1838 ($[M-H-C_6H_8O_6-CO_2]^-$), 134.0125 ($[M-H-C_6H_8O_6-C_2H_3O_2]^-$)	Methylation and glucuronidation of C1	+	+	+	+	+	−	+
C9	16.237	$C_{16}H_{20}O_{10}$	371.3198	371.2193	−0.27	371.2193 ($[M-H]^-$), 195.3327 ($[M-H-C_6H_8O_6]^-$)	Methylation, glucuronidation of C1 and reduction	+	−	−	+	−	−	+
C10	13.228	$C_{20}H_{27}NO_{11}S$	488.4912	488.5079	0.03	488.5079 ($[M-H]^-$), 387.3297 ($[M-H-C_4H_7NO_2]^-$), 367.3683	Methylation and cysteine conjugation	−	+	+	+	+	+	+

(*continued on next page*)

Table 2 (*continued*)

No.	Retention time (min)	Formula	$[M-H]^-$ (*m/z*)			MS/MS fragment ion	Metabolic pathway	Real samples						
			Theoretical	Experimental	Error (mDa)			Feces		Plasma			Urine	
								0–4 h	4–8 h	0.5 h	4 h	8 h	0–4 h	4–8 h
						([M−H−$C_3H_7NO_2S$]$^-$), 191.2087 ([M−H−$C_3H_7NO_2S$−$C_{10}H_8O_3$]$^-$), 181.0788 ([M−H−$C_3H_7NO_2S$−$C_7H_6O_6$]$^-$), 120.0823 ([M−H−$C_{17}H_{20}O_9$]$^-$)								
C11	11.803	$C_{20}H_{27}N_3O_{10}S$	500.5053	500.2758	−0.46	500.2758 ([M−H]$^-$), 320.8935 ([M−H−$C_9H_7O_4$]$^-$), 303.2319 ([M−H−$C_9H_7O_4$−H_2O]$^-$)	Methylation and glutathione Michael addition of C1	−	−	−	−	−	−	+
C12	12.118	$C_{22}H_{30}N_2O_{12}S$	545.5430	545.5468	0.01	545.5468 ([M−H]$^-$), 367.0912 ([M−H−$C_5H_8O_3N_2S$−2H]$^-$), 191.3247 ([M−H−$C_5H_8O_3N_2S$−$C_{10}H_{10}O_3$]$^-$), 93.2103 ([M−H−$C_5H_8O_3N_2S$−CH_3−$C_7H_{10}O_6$−$C_3H_3O_2$)$^-$]), 85.0024 ([M−H−$C_5H_8O_3N_2S$−$C_{10}H_9O_3$−$C_3H_7O_4$]$^-$)	Methylation and cysteinylglycine conjugation of C1	+	+	+	+	+	+	+

+: detected; −: not detected.

temperature. Fig. S4B shows that the recovery did not change significantly, indicating that the material has excellent stability. Therefore, the developed Fe_3O_4@SW-MIL-101-NH_2 could be a green and stable adsorbent.

3.5. Application in rat metabolism study

CA and its metabolites, after MSPE treatment, were analyzed using UPLC-Q-TOF-MS/MS with an ESI source in the negative ion mode. Based on an attentive study of the fragmentation behaviors, retention time, and comparison with literature data and some reference compounds (Supplementary data), the parent compound CA (C0) and its fifteen metabolites (C1–C12) were identified and detected in different metabolite samples. The retention time, major product ions, metabolic type, and test results of the different samples are summarized in Table 2. The related MS and MS/MS spectra of the parent compound and its metabolites are shown in Figs. S5 and S6.

C0 was confirmed as CA by comparing the retention time (15.952 min), experimental MS at *m/z* 353.1407 $[M-H]^-$, and the MS/MS spectra with the reference compound. The MS/MS fragment

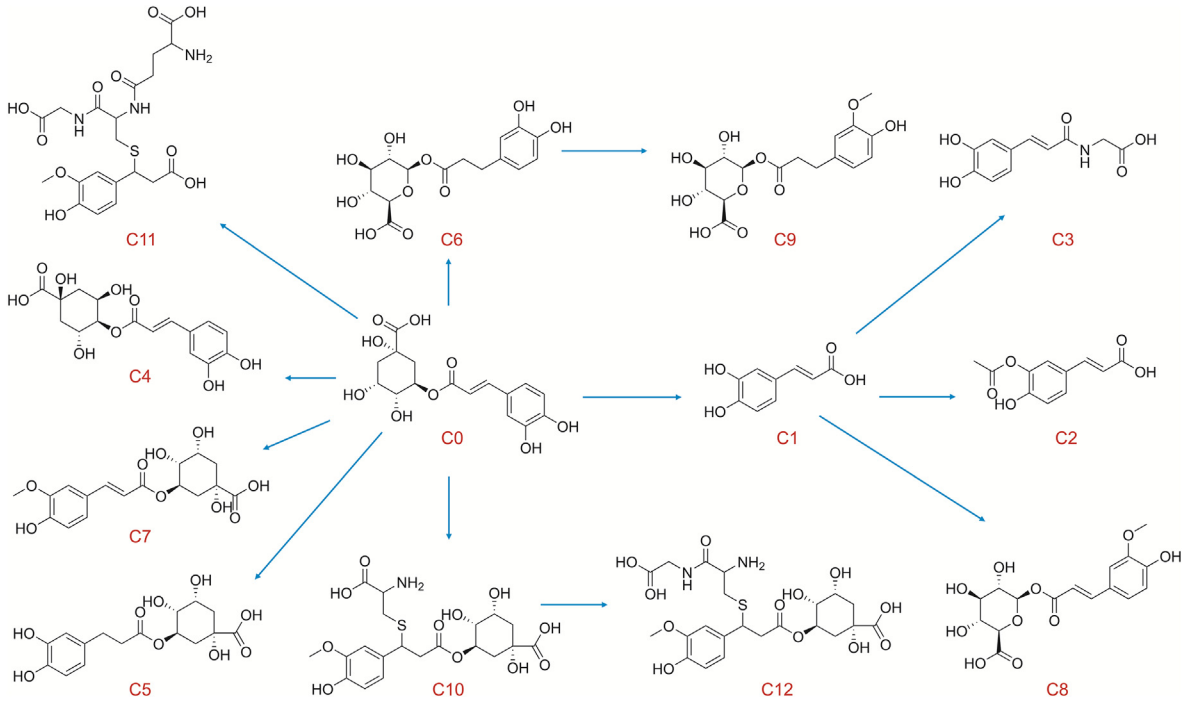

Fig. 4. Proposed biotransformation pathways of chlorogenic acid in rat. C0–C12 are the same as those in Table 2.

Table 3
Comparison of the developed method with other reported metabolic sample pretreatment methods.

Pretreatment method	Extraction conditions	Analytical method	Time (min)	Application	Sample	Refs.
LLE	100 μL of sample and 300 μL of acetonitrile	UPLC-Q-TOF MS	>20	Quercetin-3-*O*-β-D-glucopyranosyl-(4–1)-α-L-rhamnoside metabolites	Rat plasma, urine, and bile	[44]
LLE	Dilute 200 mL of sample and $CHCl_3$ (600 mL)-*n*-BuOH (600 mL)	HPLC-SPE-NMR coupled with HPLC-HRESIMS	–	Sinisan metabolites	Rat urine	[45]
SPE	0.5 mL of sample eluted with 3.2 mL of MeOH	UPLC-ESI-Q-TOF MS	–	Radix Paeoniae Alba extract metabolites	Rat bile, plasma, and urine	[46]
MMIP	100 mg of feces eluted with methanol	LC-LTQ-Orbitrap-MS	73	*Panax notoginseng* metabolites	Rat feces	[47]
MSPE	5 mL of sample-20 mg of HCP/Fe_3O_4 eluted with 2 mL of ACN	LC-MS/MS	10	Nitrofuran metabolites	Honey	[48]
MSPE	20 mg of magnetic COFs eluted with 5 mL of MeOH	LC-MS/MS	29	Aromatic amine metabolites	Human urine	[49]
MSPE	1.0 mL of sample and 2.0 mg of adsorbent eluted with mixed solution containing 0.8 mL of Na_3PO_4 (50 mM) and 0.2 mL of MeOH	UPLC-Q-TOF MS/MS	12.5	Chlorogenic acid metabolites	Rat plasma, urine, and feces	This work

COFs: covalent organic frameworks; HCP: hypercrosslinked polystyrene; HPLC-HRESIMS: high performance liquid chromatography-high resolution electrospray ionization mass spectrometry; HPLC-SPE-NMR: high performance liquid chromatography-solid phase extraction- nuclear magnetic resonance; LC-LTQ-Orbitrap-MS: liquid chromatography-linear ion trap-orbitrap mass spectrometry; LC-MS/MS: liquid chromatography-tandem mass spectrometry; LLE: liquid-liquid extraction; MMIP: magnetic molecular imprinting; MSPE: magnetic solid-phase extraction; UPLC-ESI-Q-TOF MS: ultra-performance liquid chromatography-electrospray ionization with quadrupole time-of-flight tandem mass spectrometry; SPE: solid phase extraction.

ion at *m/z* 190.9291 ([quinic acid−H]$^-$) was yielded by the breaking of the ester bond and *m/z* 178.9049 ([caffeic acid−H]$^-$) is the break of the C–O bond. Furthermore, CA produces characteristic secondary generation product ions at *m/z* 135.1120, which are formed by the neutral loss of 44 Da (CO_2) from the ion at *m/z* 178.9049. For the identification of other metabolites, please refer to Supplementary data. The identification results indicated that glucuronidation, reduction, methylation, and hydrolysis are the principal metabolic pathways of CA, and the proposed metabolic pathways are shown in Fig. 4.

3.6. Adsorption mechanism

The extraction efficiency of Fe_3O_4 and the prepared Fe_3O_4@SW-MIL-101-NH_2 were compared, and it was found that sandwich-structured materials played a major role in the extraction process. This can be attributed to the following facts: 1) both the ligand H_2BDC-NH_2 and CA contain benzene ring structures that can generate a strong π stacking interaction. 2) CA and its isomers and metabolites contain abundant carboxyl and hydroxyl groups, leading to the formation of hydrogen bonds with the amino groups of the prepared material. When the pH is decreased and free hydrogen ions are increased, flexible free hydrogen ions can overlay the electronegative atoms, resulting in a loss of hydrogen bonding. Therefore, the highest extraction efficiency was achieved at pH 5.0, proving the existence of hydrogen bonding. 3) Previous studies have shown that Fe^{3+} can chelate with CA to form an Fe^{3+}-CA complex. When phosphate was added to compete with the chelation site, the adsorption efficiency was significantly decreased, proving that chelation played a significant role in the extraction process.

3.7. Comparison with previous methods

The sample pretreatment method is an essential link in the quality analysis process, which determines the accuracy and reproducibility of the analytical results [43]. Some of the previously reported pretreatment methods for biological samples in metabolic studies, including SPE, liquid-liquid extraction, MSPE, and magnetic molecular imprinting, are summarized in Table 3 [44–49]. In this study, MSPE was employed for the first time as a preparation method for the determination of CA metabolites in biological samples. Compared with other methods, the present method, based on the high-efficiency adsorbent Fe_3O_4@SW-MIL-101-NH_2, has advantages, such as short analysis time, low organic solvent consumption, and high specificity.

4. Conclusion

In summary, a sensitive and selective pretreatment and determination method for CA metabolites in rat plasma, urine, and fecal samples is proposed. In this method, new sandwich-structured Fe-based MOF magnetic nanoparticles, which are easy to prepare, have a large specific surface area, sufficient magnetic properties, satisfactory chemical and mechanical stability, and good selectivity, were synthesized and characterized. Through the pretreatment process based on Fe_3O_4@SW-MIL-101-NH_2, the primary metabolites of CA were identified, and metabolic pathways such as reduction and methylation were proposed. In short, MSPE/UPLC-Q-TOF MS/MS can be employed as an alternative approach for the pretreatment and analysis of CA metabolites in rat biological samples.

CRediT author statement

Shi-Jun Yin: Conceptualization, Methodology, Investigation, Writing - Original draft; **Xi Zhou:** Investigation; **Li-Jing Peng:** Investigation; **Fang Li:** Investigation; **Guo-Can Zheng:** Investigation; **Feng-Qing Yang:** Supervision, Project administration, Funding acquisition; **Yuan-Jia Hu:** Supervision, Funding acquisition.

Declaration of competing interest

The authors declare that there are no conflicts of interest.

Acknowledgments

This work was sponsored by the Natural Science Foundation of Chongqing, China (Grant No.: cstc2019jcyj-msxmX0074) and was supported by the University of Macau (Grant No.: MYRG2019-00011-ICMS).

Appendix A. Supplementary data

Supplementary data to this article can be found online at https://doi.org/10.1016/j.jpha.2022.01.002.

References

[1] N. Nakatani, S. Kayano, H. Kikuzaki, et al., Identification, quantitative determination, and antioxidative activities of chlorogenic acid isomers in prune (*Prunus domestica* L.), J. Agric. Food Chem. 48 (2000) 5512–5516.

[2] C. Piñeros-Niño, C.-E. Narváez-Cuenca, A.C. Kushalappa, et al., Hydroxycinnamic acids in cooked potato tubers from Solanum tuberosum group Phureja, Food Sci. Nutr. 5 (2016) 380–389.

[3] N. Li, X.-Y. Gao, Q. Fan, et al., Rapid determination of chlorogenic acid in aqueous solution of Flos Lonicerae Japonicae extraction, Zhongguo Zhongyao Zazhi 32 (2007) 312–314.

[4] K. Arai, H. Terashima, S. Aizawa, et al., Simultaneous determination of trigonelline, caffeine, chlorogenic acid and their related compounds in instant coffee samples by HPLC using an acidic mobile phase containing octanesulfonate, Anal. Sci. 31 (2015) 831–835.

[5] Y. Sato, S. Itagaki, T. Kurokawa, et al., In vitro and in vivo antioxidant properties of chlorogenic acid and caffeic acid, Int. J. Pharm. 403 (2011) 136–138.

[6] Q. Li, Y. Zhao, X. Zheng, et al., Chlorogenic acid alters the biological characteristics of basophil granulocytes by affecting the fluidity of the cell membrane and triggering pseudoallergic reactions, Int. J. Mol. Med. 32 (2013) 1273–1280.

[7] L.-N. Xing, M.-M. Zhou, Y. Li, et al., Recent progress of potential effects and mechanisms of chlorogenic acid and its intestinal metabolites on central nervous system diseases, Zhongguo Zhongyao Zazhi 40 (2015) 1044–1047.

[8] A. Suzuki, A. Fujii, N. Yamamoto, et al., Improvement of hypertension and vascular dysfunction by hydroxyhydroquinone-free coffee in a genetic model of hypertension, FEBS Lett. 580 (2006) 2317–2322.

[9] K. Yamagata, Y. Izawa, D. Onodera, et al., Chlorogenic acid regulates apoptosis and stem cell marker-related gene expression in A549 human lung cancer cells, Mol. Cell. Biochem. 441 (2018) 9–19.

[10] B. McDougall, P.J. King, B.W. Wu, et al., Dicaffeoylquinic and dicaffeoyltartaric acids are selective inhibitors of human immunodeficiency virus type 1 integrase, Antimicrob. Agents Chemother. 42 (1998) 140–146.

[11] M.G.S. Palmieri, L.T. Cruz, F.S. Bertges, et al., Enhancement of antioxidant properties from green coffee as promising ingredient for food and cosmetic industries, Biocatal. Agric. Biotechnol. 16 (2018) 43–48.

[12] J. Li, S.-P. Wang, Y.-Q. Wang, et al., Comparative metabolism study on chlorogenic acid, cryptochlorogenic acid and neochlorogenic acid using UHPLC-Q-TOF MS coupled with network pharmacology, Chin. J. Nat. Med. 19 (2021) 212–224.

[13] H. Shen, X. Song, Y. Zhang, et al., Profiling of brevetoxin metabolites produced by *Karenia brevis* 165 based on liquid chromatography-mass spectrometry, Toxins 13 (2021), 354.

[14] A. Abraham, Y. Wang, K.R. El Said, et al., Characterization of brevetoxin metabolism in Karenia brevis bloom-exposed clams (*Mercenaria* sp.) by LC-MS/MS, Toxicon 60 (2012) 1030–1040.

[15] R.H. Pierce, M.S. Henry, L.S. Proffitt, et al., Evaluation of solid sorbents for the recovery of polyether toxins (brevetoxins) in seawater, Bull. Environ. Contam. Toxicol. 49 (1992) 479–484.

[16] S.F. Teunissen, H. Rosing, L. Brunsveld, et al., Analysis of 2-amino-1-methyl-6-phenylimidazo[4,5-*b*]pyridine and its phase I and phase II metabolites in mouse urine using LC-UV-MS-MS, Chromatographia 74 (2011) 215–226.

[17] T. Ogawa, H. Hattori, M. Iwai, et al., A rapid and simultaneous analysis of theophylline and its metabolites in human whole blood by ultra-performance liquid chromatography-tandem mass spectrometry, Forensic Toxicol. 30 (2012) 142–148.

[18] M. Majd, M. Yazdanpanah, M.R. Bayatloo, et al., Recent advances and applications of cyclodextrins in magnetic solid phase extraction, Talanta 229 (2021), 122296.

[19] H.-L. Jiang, N. Li, L. Cui, et al., Recent application of magnetic solid phase extraction for food safety analysis, Trends Anal. Chem. 120 (2019), 115632.

[20] S.-J. Yin, J. Zhao, F.-Q. Yang, Recent applications of magnetic solid phase extraction in sample preparation for phytochemical analysis, J. Pharm. Biomed. Anal. 192 (2021), 113675.

[21] Y. Liao, X. Huang, Z. Wang, et al., Research progress in the application of magnetic solid phase extraction based on carbon based magnetic materials in food analysis, Se Pu 39 (2021) 368–375.

[22] L. Xie, R. Jiang, F. Zhu, et al., Application of functionalized magnetic nanoparticles in sample preparation, Anal. Bioanal. Chem. 406 (2014) 377–399.

[23] M. Yu, L. Wang, L. Hu, et al., Recent applications of magnetic composites as extraction adsorbents for determination of environmental pollutants, Trends Anal. Chem. 119 (2019), 115611.

[24] W.-K. Li, Y.-P. Shi, Recent advances and applications of carbon nanotubes based composites in magnetic solid-phase extraction, Trends Anal. Chem. 118 (2019) 652–665.

[25] A. Speltini, M. Sturini, F. Maraschi, et al., Recent trends in the application of the newest carbonaceous materials for magnetic solid-phase extraction of environmental pollutants, Trends Environ. Analyt. Chem. 10 (2016) 11–23.

[26] Z. Meng, L. Zhang, Y. Huang, Development of metal-organic framework composites in sample pretreatment, Se Pu 36 (2018) 216–221.

[27] J. Ma, G. Wu, S. Li, et al., Magnetic solid-phase extraction of heterocyclic pesticides in environmental water samples using metal-organic frameworks coupled to high performance liquid chromatography determination, J. Chromatogr. A 1553 (2018) 57–66.

[28] Y. Wang, M. Yan, Q. Ji, et al., Fast magnetic solid-phase extraction using an Fe_3O_4-NH_2@MOF material for monohydroxy polycyclic aromatic hydrocarbons in urine of coke-oven workers, Anal. Methods 12 (2020) 2872–2880.

[29] H. Duo, X. Lu, S. Wang, et al., Synthesis of magnetic metal-organic framework composites, Fe_3O_4-NH_2@MOF-235, for the magnetic solid-phase extraction of benzoylurea insecticides from honey, fruit juice and tap water samples, New J. Chem. 43 (2019) 12563–12569.

[30] Y. Li, X. Zhou, L. Dong, et al., Magnetic metal-organic frameworks nanocomposites for negligible-depletion solid-phase extraction of freely dissolved polyaromatic hydrocarbons, Environ. Pollut. 252 (2019) 1574–1581.

[31] T. Wan, W. Li, Z. Chen, Metal organic framework-801 based magnetic solid-phase extraction and its application in analysis of preterm labor treatment drugs, J. Pharm. Biomed. Anal. 199 (2021), 114049.

[32] S.-H. Huo, H.-Y. An, J. Yu, et al., Pyrolytic in situ magnetization of metal-organic framework MIL-100 for magnetic solid-phase extraction, J. Chromatogr. A 1517 (2017) 18–25.

[33] R. Yang, J. Tian, Y. Liu, et al., Interaction mechanism of ferritin protein with chlorogenic acid and iron ion: the structure, iron redox, and polymerization evaluation, Food Chem. 349 (2021), 129144.

[34] Y. Kono, S. Kashine, T. Yoneyama, et al., Iron chelation by chlorogenic acid as a natural antioxidant, Biosci. Biotechnol. Biochem. 62 (1998) 22–27.

[35] J. Guo, Y. Wan, Y. Zhu, et al., Advanced photocatalysts based on metal nanoparticle/metal-organic framework composites, Nano Res. 14 (2021) 2037–2052.

[36] M. Musa, W.A. Wan Lbrahim, F. Mohd Marsin, et al., Graphene-magnetite as adsorbent for magnetic solid phase extraction of 4-hydroxybenzoic acid and 3, 4-dihydroxybenzoic acid in stingless bee honey, Food Chem. 265 (2018) 165–172.

[37] M. Liu, Q. Huang, L. Li, et al., Cerium-doped MIL-101-NH_2(Fe) as superior adsorbent for simultaneous capture of phosphate and As(V) from Yangzonghai coastal spring water, J. Hazard Mater. 423 (2021), 126981.

[38] P.S. Gao, Y. Guo, X. Li, et al., Magnetic solid phase extraction of sulfonamides based on carboxylated magnetic graphene oxide nanoparticles in environmental waters, J. Chromatogr. A 1575 (2018) 1–10.

[39] F. Aflatouni, M. Soleimani, Preparation of a new polymerized ionic liquid-modified magnetic nano adsorbent for the extraction and preconcentration of nitrate and nitrite anions from environmental water samples, Chromatographia 81 (2018) 1475–1486.

[40] C. Huang, J. Wang, M. Li, et al., Construction of a novel Z-scheme V_2O_5/NH_2-MIL-101(Fe) composite photocatalyst with enhanced photocatalytic degradation of tetracycline, Solid State Sci. 117 (2021), 106611.

[41] Ş.S. Bayazit, S.T. Danalıoğlu, M.A. Salam, et al., Preparation of magnetic MIL-101 (Cr) for efficient removal of ciprofloxacin, Environ. Sci. Pollut. Res. 24 (2017) 25452–25461.

[42] P. Zhu, X.-L. Miao, Y. Chen, Degradation kinetics of chlorogenic acid, cryptochlorogenic acid, and neochlorogenic acid at neutral and alkaline pH values, Yao Xue Xue Bao 51 (2016) 122–126.

[43] X. Jing, H. Wang, X. Huang, et al., Digital image colorimetry detection of carbaryl in food samples based on liquid phase microextraction coupled with a microfluidic thread-based analytical device, Food Chem. 337 (2021), 127971.

[44] X. Yao, G.-S. Zhou, Y.-P. Tang, et al., Quercetin-3-*O*-β-D-glucopyranosyl-(4→1)-α-L-rhamnoside metabolites in the rat using UPLC-Q-TOF/MS, Chin. J. Nat. Med. 12 (2014) 705–711.

[45] Y.-P. Lee, T.-F. Kuo, S.-S. Lee, Identification of the metabolites of TCM prescription Sinisan, found in miniature pig urine via intragastric administration, J. Pharm. Biomed. Anal. 111 (2015) 311–319.

[46] Z.-W. Chen, L. Tong, S.-M. Li, et al., Identification of metabolites of Radix Paeoniae Alba extract in rat bile, plasma and urine by ultra-performance liquid chromatography-quadrupole time-of-flight mass spectrometry, J. Pharm. Anal. 4 (2014) 14–25.

[47] Q. Cai, Z. Yang, N. Chen, et al., Selective capture and rapid identification of Panax notoginseng metabolites in rat faeces by the integration of magnetic molecularly imprinted polymers and high-performance liquid chromatography coupled with orbitrap mass spectrometry, J. Chromatogr. A 1455 (2016) 65–73.

[48] A.O. Melekhin, V.V. Tolmacheva, E.G. Shubina, et al., Determination of nitrofuran metabolites in honey using a new derivatization reagent, magnetic solid-phase extraction and LC-MS/MS, Talanta 230 (2021), 122310.

[49] J. Yu, B. Wang, J. Cai, et al., Selective extraction and determination of aromatic amine metabolites in urine samples by using magnetic covalent framework nanocomposites and HPLC-MS, RSC Adv. 10 (2020) 28437–28446.